NANO EXPRESS

Fabrication of Worm-Like Nanorods and Ultrafine Nanospheres of Silver Via Solid-State Photochemical Decomposition

S. Navaladian · B. Viswanathan · T. K. Varadarajan ·
R. P. Viswanath

Abstract Worm-like nanorods and nanospheres of silver have been synthesized by photochemical decomposition of silver oxalate in water by UV irradiation in the presence of CTAB and PVP, respectively. No external seeds have been employed for the synthesis of Ag nanorods. The synthesized Ag colloids have been characterized by UV-visible spectra, powder XRD, HRTEM, and selected area electron diffraction (SAED). Ag nanospheres of average size around 2 nm have been obtained in the presence of PVP. XRD and TEM analyses revealed that top and basal planes of nanorods are bound with {111} facets. Williamson–Hall plot has revealed the presence of defects in the Ag nanospheres and nanorods. Formation of defective Ag nanocrystals is attributed to the heating effect of UV-visible irradiation.

Keywords Ag nanorods · Nanospheres · CTAB · PVP · Photochemical decomposition · WH plot

Introduction

Silver nanoparticles have been known for the variety of applications in various fields such as catalysis, electronics, optics, medicine, and environment. Particularly, Ag nanoparticles find applications in diagnostic biomedical optical imaging [1], molecular labeling [2], spectrally selective coating for the solar energy absorption [3], cancer therapy [4], and sensors for refractive index [5], and ammonia [6].

Moreover, Ag nanoparticles are known for the antimicrobial [7], surface-enhanced Raman scattering (SERS) [8] and metal-enhanced fluorescence properties [9]. Silver nanoparticles are also known for cytoprotective and post-infected anti-HIV-1 activities [10]. Ag nanorods have been synthesized by arc discharge technique [11], polyol process [12], hard template synthesis using porous materials such as mesoporous silica [13], and carbon nanotubes [14], using surfactants such as cetyl trimethyl ammonium bromide (CTAB) [15], sodium dodecyl sulfonate [16], and dodecyl benzene sulfonic acid sodium (DBS) [17], seed-mediated [15] and seedless, and surfactantless wet chemical approach [18]. Even though various methods have been known, the facile, quick, and the cost-effective synthetic routes are still elusive. Since compounds of silver like silver oxalate $(Ag_2C_2O_4)$ are photosensitive and yield metallic silver upon the exposure to UV light, those compounds can be photochemically decomposed to obtain Ag nanoparticles in the presence of capping agents. Synthesis of Ag nanoparticles from silver oxalate by thermal and microwave-assisted decomposition has been reported, as temperature needed for the decomposition of silver oxalate is as low as 140 °C [19, 20]. In this article, a fast synthesis of Ag nanospheres and nanorods by UV irradiation of silver oxalate in the presence of poly (vinyl pyrrolidone) (PVP) and cetyl trimethyl ammonium bromide (CTAB) as capping agents has been demonstrated.

S. Navaladian · B. Viswanathan · T. K. Varadarajan ·
R. P. Viswanath (✉)
National Centre for Catalysis Research, Department
of Chemistry, Indian Institute of Technology Madras,
Chennai 600 036, India
e-mail: rpviswanath@gmail.com

Experimental Details

Synthesis of Silver Oxalate

Silver oxalate was prepared by mixing the solutions of 50 mL of 0.5 M AgNO₃ (Merck, 99.9%) and 30 mL of

0.5 M oxalic acid (SRL, India, 99.8%) [21]. The white precipitate formed was filtered, washed with distilled water, dried in an air oven for 1 h, and stored in a dark bottle.

Synthesis of Ag Nanospheres and Nanorods

In a typical synthesis, 0.1 g of PVP ($M.w \approx 40,000$, SRL, India, 99%) and 0.02 g of $Ag_2C_2O_4$ were stirred in 20 mL of doubly distilled water in a quartz tube for 15 min in the dark and purged with N_2 gas for 5 min followed by the UV irradiation using a 450 W Hg lamp (Oriel Corporation, USA) for 10 min. A pale yellow colloid was formed. During the irradiation, no cut-off filter was used. The resulting colloids were washed by centrifugation at 6000 rpm for TEM analysis. The same procedure was adopted for the CTAB-based synthesis of Ag colloids (Fluka, ≥99%). The ratios of $Ag_2C_2O_4$ and CTAB used for the synthesis are 1:2, 1:5, and 1:8(w/w). The color of the colloids was yellow, blue, and black, respectively.

Characterization

UV-visible diffused reflectance spectrum (DRS) of silver oxalate was recorded using Thermo scientific Evolution 600 UV-visible spectrophotometer. The surface morphology of silver oxalate was analyzed with a FEI (Model: Quanta 200) scanning electron microscope operating at 30 kV. UV-visible spectra of silver colloids were recorded using Jasco V-530 spectrophotometer. HRTEM analyses were carried out using JEOL-3010 transmission electron microscopes working at 300 kV and Philips CM20 transmission electron microscope (TEM) with EDX mapping working at 200 kV. Samples for TEM analysis were prepared by dispersing Ag nanoparticles in ethanol followed by drop casting on a copper grid (400 mesh) coated with carbon film. Powder XRD patterns were recorded using a SHIMADZU XD-D1 diffractometer using Ni-filtered Cu K_α radiation ($\lambda = 1.5406$ Å) at the scan rate of 0.1°/s. To correct the instrumental broadening, Si standard was used.

Results and Discussion

As-synthesized $Ag_2C_2O_4$ has been confirmed by using XRD and TGA [20]. UV-visible diffuse reflectance spectrum of $Ag_2C_2O_4$ is shown in Fig. 1. A sharp absorption peak at 285 nm and two humps at 323 nm and 343 nm are observed in the spectrum. This indicates that $Ag_2C_2O_4$ absorbs in the UV region. The band gap of as-synthesized $Ag_2C_2O_4$ has been found to be 4.35 eV. SEM image of
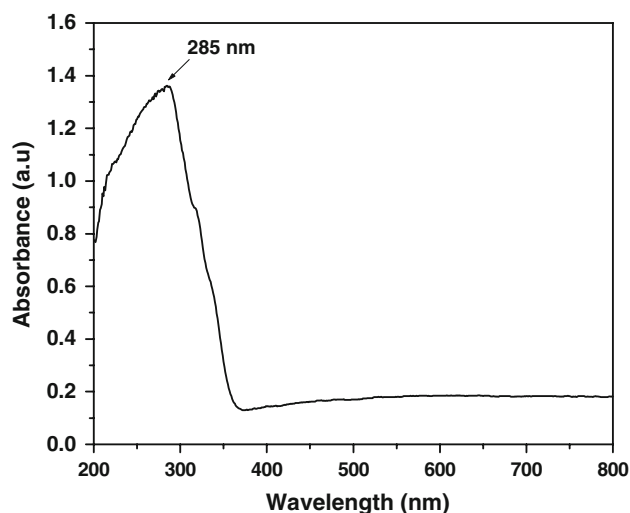

Fig. 1 UV-visible DRS of as-synthesized silver oxalate

$Ag_2C_2O_4$ given in Fig. 2 shows irregular shaped particles of size in the range of 0.5–7.5 μm.

UV-visible spectra of synthesized Ag colloids are given in Fig. 3. UV-visible spectrum of Ag colloid synthesized using 1:5 of $Ag_2C_2O_4$ and PVP shows a single sharp SPR band centered at around 404 nm. This single sharp SPR band indicates the presence of spherical Ag nanoparticles with average size below 10 nm in the colloid [19]. The corresponding HRTEM images given in Fig. 4a, b shows highly dispersed Ag nanoparticles on the grid. Size of the Ag particles lies between 1 and 6 nm and the average size of Ag nanoparticles is around 2 nm. The lattice-resolved image of a single Ag nanoparticle (6.2 × 7.2 nm) given in Fig. 4c shows the cubic arrangement with inter planar
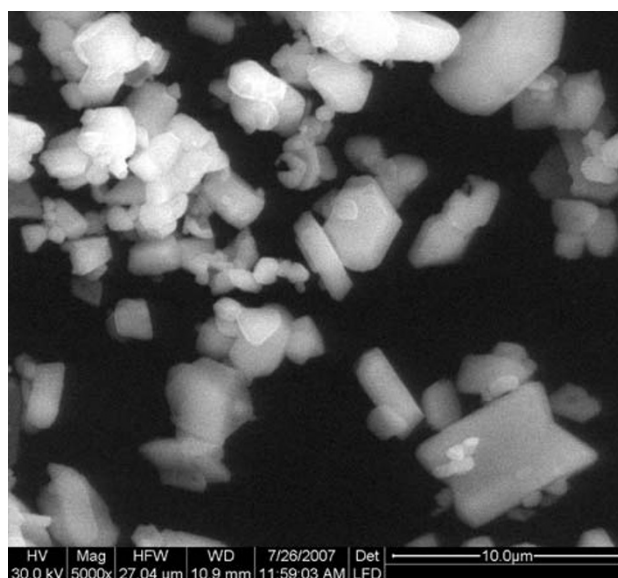

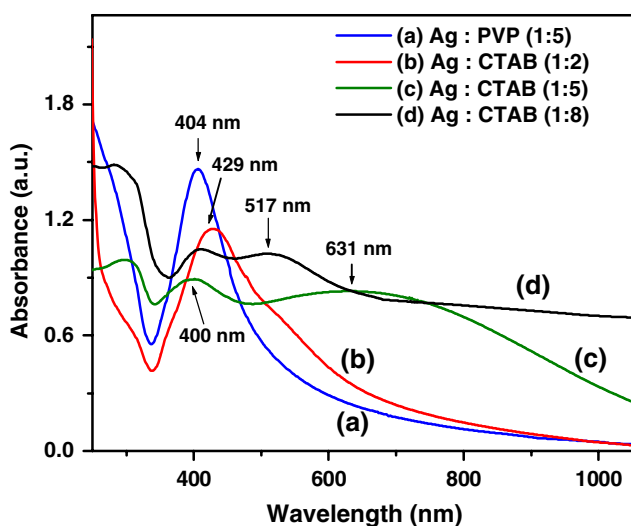**Fig. 2** SEM image of as-synthesized silver oxalate

Fig. 3 UV-visible spectra of Ag colloids synthesized by photochemical decomposition of silver oxalate using PVP and CTAB as capping agents
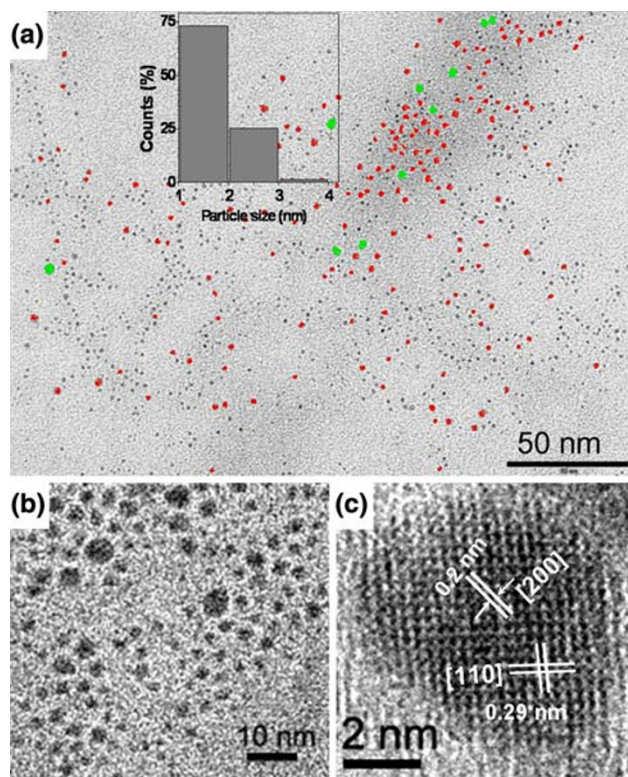

Fig. 4 a EDX-mapped TEM image (green: 3–4 nm; red: 2–3 nm; black: <2 nm) **b** HRTEM image, and **c** lattice-resolved HRTEM image of Ag nanoparticles synthesized using 1:5 ratio of $Ag_2C_2O_4$ and PVP

d-spacings of 0.2 and 0.288 nm; these d values correspond to (200) and (110) planes of Ag metal, respectively. Hence, the exposed face is bound with (100) facet. These observations confirm the presence of silver in fcc arrangement.

Since synthesis of fine and narrow dispersed particles has been achieved with 1:5 ratio of $Ag_2C_2O_4$ and PVP, further studies based on varying the ratio of $Ag_2C_2O_4$ and PVP have not been carried out.

In the case of 1:2 ratio of $Ag_2C_2O_4$ and CTAB, a single broad SPR band observed with λ_{max} at 429 nm indicates the presence of Ag particles with the wide distribution of size or anisotropic Ag nanoparticles [20, 22]. The corresponding HRTEM image is shown in Fig. 5, which shows the presence of spherical and quasi-spherical Ag nanoparticles with size in the range of 4–62 nm. Average size of Ag nanospheres is ∼30 nm. Lattice-resolved images (Fig. 5b and c) of single Ag nanospheres show lattice fringes corresponding to (111) plane of Ag metal. SAED pattern of a Ag nanosphere given in Fig. 5d shows spots and the rings composed of spots. This pattern implies the polycrystalline nature of Ag nanospheres. The spots as well as rings are indexed to (111), (200), (220), (311), (222), (400), (331), (420), and (422) planes of silver with fcc structure (JCPDS file - 89-3722).

UV-visible spectrum corresponding to Ag colloid formed using 1:5 ratio of $Ag_2C_2O_4$ and CTAB shows a couple of SPR bands with λ_{max} at 400 and 631 nm. This implies the presence of anisotropic nanoparticles like nanorods and Ag spherical particles. SPR bands at 400 nm and at 631 nm correspond to transverse interaction and another to longitudinal interaction, respectively, of anisotropic Ag nanoparticles like rods with visible light [15, 23]. The corresponding HRTEM images in Fig. 6a, b show the presence of nanorods and anisotropic particles. The length of the nanorods is up to 61 nm and the aspect ratio of nanorods varies from 2 to 6. The nanorods are not uniform in thickness, non-straight, and consist of particles at the edge. The average thickness of Ag nanorods is around 6 nm. Some of the rods appear to have formed through the attachment of the particles. Lattice-resolved HRTEM image of the Ag nanorod is shown in Fig. 6c. Lattice fringes with a d value of 0.25 nm is observed at the middle part of the rod. This corresponds to 1/3{422} reflection of silver with fcc structure. In general, appearance of 1/3{422} reflection is forbidden for the perfect single crystalline fcc lattice. However, it is observed only in the case of nanoplates or thin films of Au and Ag metals bound by atomically flat surfaces [24]. The corresponding SAED pattern, recorded in the direction perpendicular to the surface of Ag nanorod, shows spots. This pattern reveals that middle part of Ag nanorod is single crystalline. The symmetric hexagonal spots observed are indexed to {220}, {331}, and {422} reflections. These observations, too, reveal that top and basal planes of the nanorod are bound with {111} facets [25]. A line in Fig. 6c indicates the presence of twin boundaries parallel to rod. At the edge of the nanorod, a particle with lattice fringes corresponding to

Fig. 5 a HRTEM image, **b** and **c** lattice-resolved HRTEM images, and **d** SAED pattern of a Ag nanosphere synthesized using 1:2 ratio of $Ag_2C_2O_4$ and CTAB
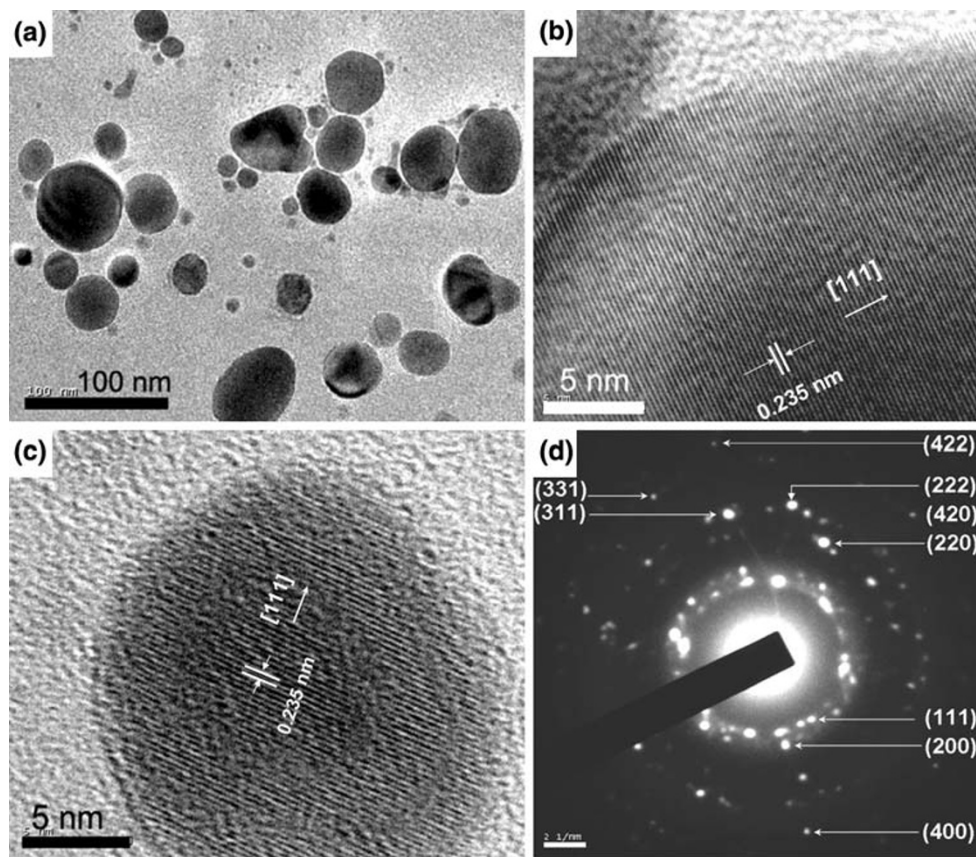

(200) plane of Ag with *fcc* structure is observed. This shows that the nanorod has originated from the particle and hence the rod, as a whole, is polycrystalline. This observation implies that particles act as seeds for the formation of nanorods. In the case of 1:8 ratio of $Ag_2C_2O_4$ and CTAB, UV-visible spectrum shows SPR bands at 409, 517, and 725 nm, revealing the presence of anisotropic Ag nanoparticles. The corresponding HRTEM in Fig. 7 shows the presence of featureless nanorods. In Fig. 7b, a nanorod with diameter of ~ 44 nm and aspect ratio of around 5 is observed. In this case too, a particle is present at the end of the nanorod. However, the formation of monodispersed nanorods has not been achieved in the case of 1:8 ratio of $Ag_2C_2O_4$ and CTAB. Hence, it is clear that only 1:5 ratio of $Ag_2C_2O_4$ and CTAB is better optimal ratio to form nanorods than 1:2 and 1:8 ratios.

In order to understand the intermediate stage of the reaction, reaction mixture (1:8 ratio of $Ag_2C_2O_4$ and CTAB) has been analyzed by HRTEM after 5 min of UV irradiation. The corresponding TEM images in Fig. 7c, d show the decomposed surface of $Ag_2C_2O_4$ decorated with Ag nanoparticles. The contrast between Ag metal core and $Ag_2C_2O_4$ compound is clearly seen from Fig. 7d. However, after 10 min of irradiation, no $Ag_2C_2O_4$ has been observed. This shows that 10 min of UV-irradiation is enough for

complete decomposition of $Ag_2C_2O_4$ dispersed in the solution. The decomposition of $Ag_2C_2O_4$ is so rapid because the intensity of UV lamp employed is high.

XRD powder patterns of Ag nanospheres and Ag nanorods are shown in Fig. 8. The inter planar *d*-spacing of XRD peaks correspond to (111), (200), (220), (311), and (222) planes of Ag with *fcc* structure (JCPDS file no: 89-3722). Average crystallite size corresponding to each plane has been calculated from XRD patterns using Scherrer's equation [26] and given in Fig. 9. The average crystallite size of the spherical Ag nanoparticles formed using PVP lies between 2.8 and 4.7 nm. However, as per HRTEM analysis, it is around 2 nm. This deviation is mainly due to the poor scattering ability of Ag particles of size below 3 nm. The average crystallite size of Ag nanospheres synthesized using 1:2 ratio of $Ag_2C_2O_4$ and CTAB lies between 25 and 32 nm and the corresponding particle size from HRTEM lies between 4 and 62 nm. This observation indicates the polycrystalline nature of Ag nanoparticles. In the case of spherical nanoparticles, average crystallite size decreases while moving from low to high Bragg angles. This reveals the isotropic nature of the nanocrystals. In the case of Ag nanorods, the average crystallite size lies in the range between 6.4 and 10.4 nm, and particle size observed from HRTEM is higher than that from XRD analysis. This

Fig. 6 **a** and **b** HRTEM images, **c** Lattice-resolved HRTEM image, and **d** SAED pattern of the Ag nanorod synthesized using 1:5 ratio Ag$_2$C$_2$O$_4$ and CTAB. SAED pattern was recorded in the perpendicular direction to the nanorod
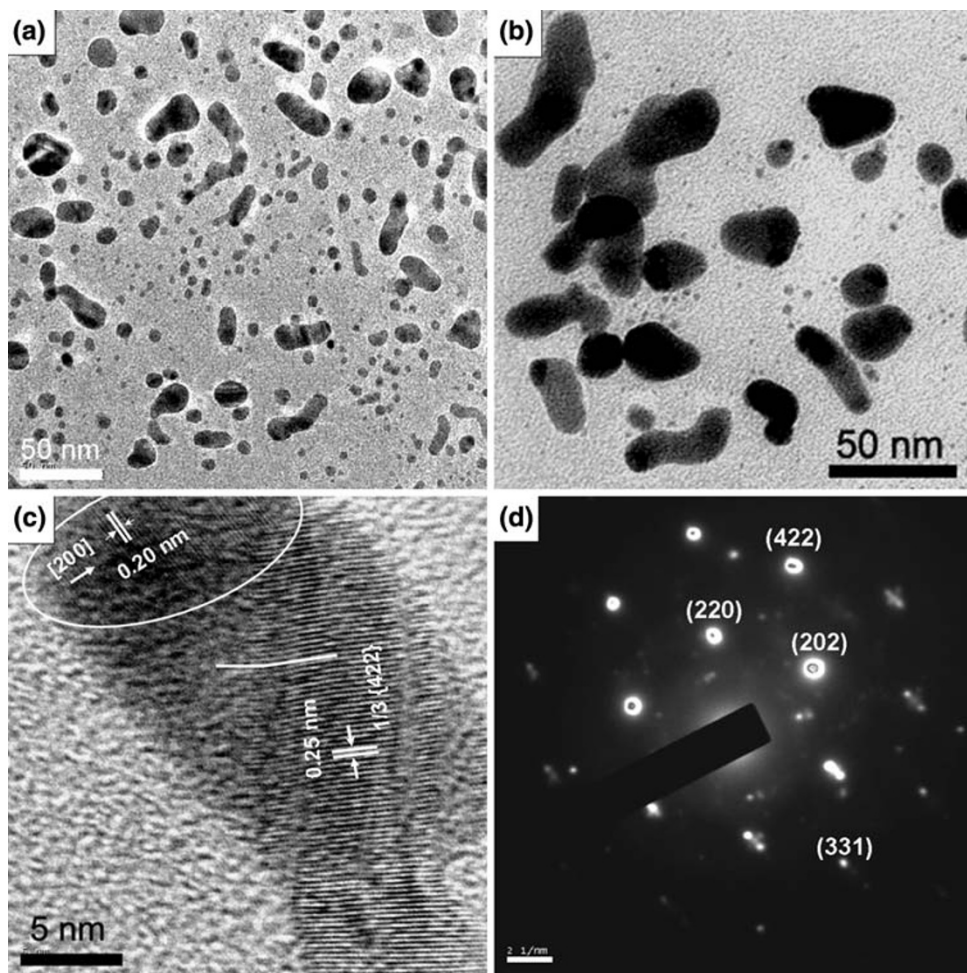
reveals that Ag nanorods are polycrystalline as evidenced by HRTEM analysis where rods contain more than one crystallite (Fig. 6b). Moreover, the average crystallite size of (111) planes considerably deviates from that of other planes. This deviation reveals the faceting in the nanocrystals. Since (111) planes show higher value of average crystallite size than that of other planes, longitudinal direction of the rods is bound with {111} planes. This observation shows good agreement with HRTEM image (Fig. 6c).

Texture coefficient corresponding to each plane in XRD pattern has been calculated by Hall method to understand the faceting in nanoparticles and shown in Fig. 10. Texture coefficient (C$_{hkl}$) has been calculated using the following Eq. 1 [27].

$$C_{(hkl)} = \frac{I_{(hkl)_i}}{I_{o(hkl)i}} \bigg/ \frac{1}{n} \sum_n \frac{I_{(hkl)_n}}{I_{o(hkl)n}} \tag{1}$$

where, $C_{(hkl)}$ is the texture coefficient of the facet (hkl), $I_{(hkl)}$ is the intensity of the (hkl) reflection of the sample under analysis, $I_{o(hkl)}$ is the intensity of the (hkl) reflection of a polycrystalline bulk sample, and 'n' is the number of reflections taken into account. By using this equation, the preferential orientation of the facets can be understood. $C_{(hkl)}$ is expected to be unity for the facet, which does not have preferential orientation. If it is higher than unity, it is a preferentially grown (highly exposed to X-ray) facet. The reference (polycrystalline bulk) used for the calculation is JCPDS file 89-3722. In the case of texture coefficient, Ag nanorods exhibit the similar trend as observed in the case of crystallite size. In other words, $C_{(111)}$ and $C_{(222)}$ are above unity and deviate from that of others. This reveals the faceting of {111} planes in Ag nanorods. In the case of both the Ag nanospheres, texture coefficients increase while moving from planes of lower to higher Bragg angle. In other words, $C_{(220)}$, $C_{(311)}$, and $C_{(222)}$ are higher than $C_{(111)}$ and $C_{(222)}$. This trend is attributed to the difference between the synthesized Ag nanospheres and polycrystalline bulk reference. This difference is due to the effect of particle size in X-ray scattering. In the case of nanospheres, peaks at higher Bragg angle shows higher intensity than in the case of bulk sample. Similar phenomenon has been observed for Pt and Pd nanoparticles [28, 29]. In fact, the particle size effect on scattering is observed within two spherical Ag nanoparticles synthesized with different sizes, where $C_{(111)}$ of smaller Ag

Fig. 7 a and **b** HRTEM images of Ag nanorods synthesized using 1:8 ratio $Ag_2C_2O_4$ and CTAB; **c** and **d** HRTEM images of intermediate reaction mixture after 5 min of UV irradiation
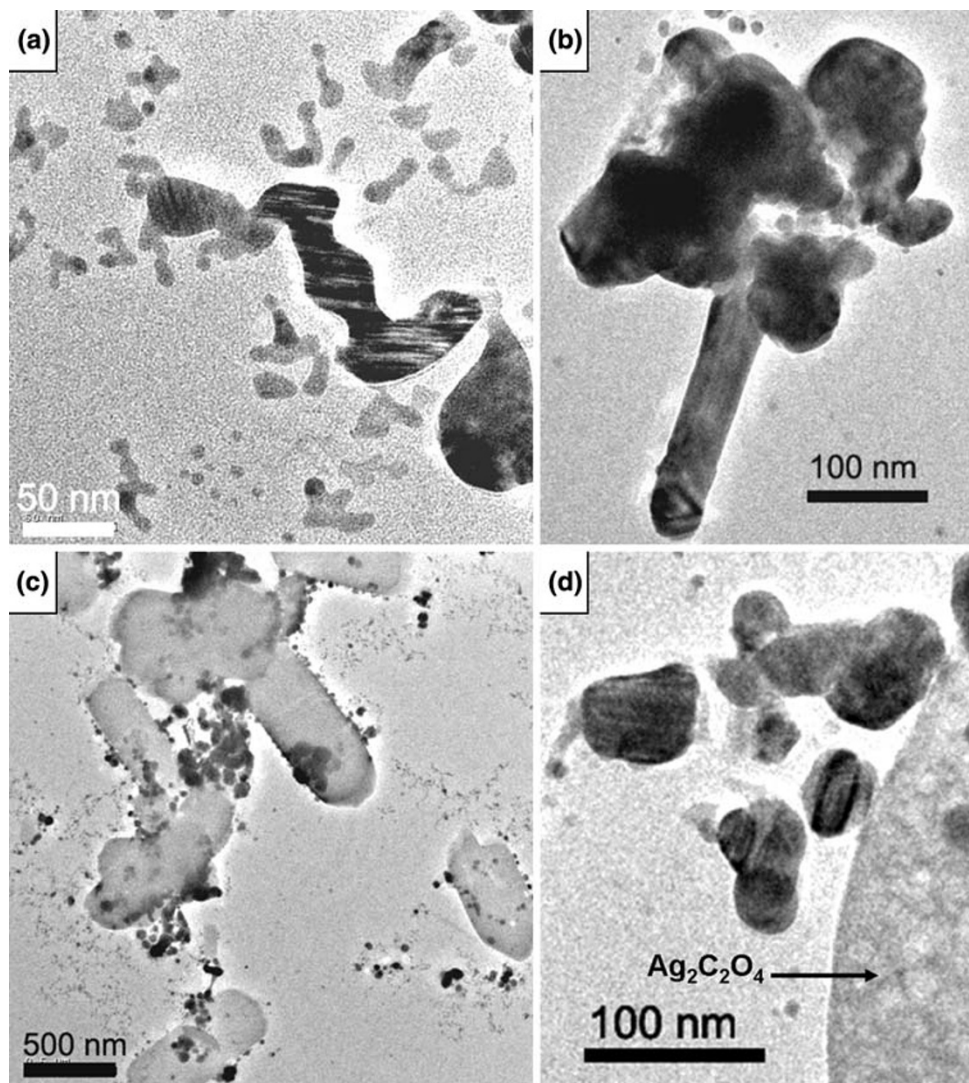
nanospheres (~ 2 nm) is lower than that of bigger Ag nanospheres (~ 30 nm). Moreover, $C_{(111)}$ of Ag nanorods is smaller than $C_{(222)}$ for the same reason.

In order to understand the contribution of strain in line broadening, line-broadening analysis was done by Williamson–Hall plot and shown in Fig. 11 [30]. Williamson–Hall (WH) plot is the plot of the integral breadth in the reciprocal space ($\Delta K = \beta \cos\theta/\lambda$, β-FWHM of XRD line) with respect to reciprocal lattice space ($K = 2\sin\theta/\lambda$). The slope corresponds to strain and the intercept corresponds to $0.9/D$ (D-crystallite size). The straight line (linear fit) was drawn using the least-square analysis. The correlation coefficient (R), the average crystallite size, and strain in lattice are given in Table 1. The R value of Ag nanocrystals are in the following order: nanospheres (~ 2 nm) < nanorods < nanospheres (~ 30 nm). The same is the order for the decrease of anisotropy in the broadening of nanocrystals. The microstrain in Ag nanocrystals are in the following

order: nanospheres (~ 2 nm) > nanorods > nanospheres (~ 30 nm). This observation indicates that the defect density is higher in the nanospheres (~ 2 nm) than in nanorods [31]. Average crystallite size calculated using WH plot for nanospheres (~ 2 nm) and nanorod is slightly higher than that from Scherrer's equation due to the contribution of strain in line broadening. This is mainly due to the defects in lattice of small Ag crystals.

Silver oxalate decomposes under UV irradiation to yield metallic silver and CO_2 gas. This is mainly owing to the high photosensitivity of $Ag_2C_2O_4$ [21]. Since this decomposition of $Ag_2C_2O_4$ is thermodynamically favorable due to the suitable reduction potentials of oxalate $\left(E^\circ_{(2CO_2/C_2O_4^{2-})} = -0.49\,\text{V}\right)$ [27] and $Ag^+\left(E^\circ_{Ag^+/Ag} = 0.79\,\text{V}\right)$ [32], decomposition occurs rapidly under UV radiation to yield metallic Ag as shown in Eq. 2.
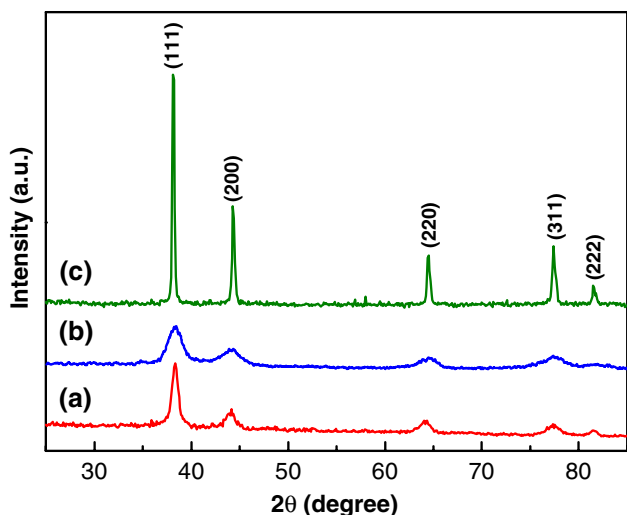
Fig. 8 Powder XRD patterns of (a) Ag nanorods synthesized using 1:5 ratio of $Ag_2C_2O_4$ and CTAB and (b) and (c) nanospheres synthesized using 1:5 ratio of $Ag_2C_2O_4$ and PVP and 1:2 ratio of $Ag_2C_2O_4$ and CTAB, respectively

Fig. 10 Texture coefficients of (a) Ag nanorods synthesized using 1:5 ratio of $Ag_2C_2O_4$ and CTAB, and (b) and (c) nanospheres synthesized using 1:5 ratio of $Ag_2C_2O_4$ and PVP and 1:2 ratio of $Ag_2C_2O_4$ and CTAB, respectively, with respect to various crystal planes
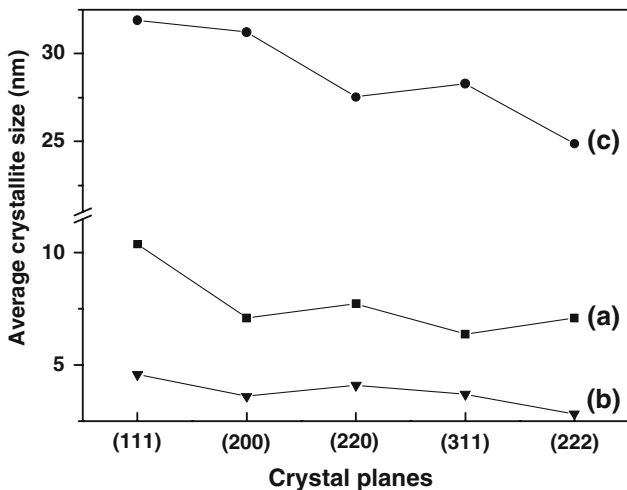

Fig. 9 Average crystallite sizes of (a) Ag nanorods synthesized using 1:5 ratio of $Ag_2C_2O_4$ and CTAB and (b) and (c) nanospheres synthesized using 1:2 ratio of $Ag_2C_2O_4$ and CTAB and 1:5 ratio of $Ag_2C_2O_4$ and PVP, respectively, with respect to various crystal planes

Fig. 11 The conventional Williamson–Hall plot for (a) Ag nanorods synthesized using 1:5 ratio of $Ag_2C_2O_4$ and CTAB, and (b) and (c) nanospheres synthesized using 1:5 ratio of $Ag_2C_2O_4$ and PVP and 1:2 ratio of $Ag_2C_2O_4$ and CTAB, respectively, with respect to various crystal planes

$$Ag_2C_2O_{4(s)} \xrightarrow{h\nu} 2Ag_{(s)} + 2CO_{2(g)} \qquad (2)$$
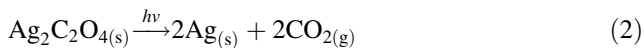
Oxalate dianion in $Ag_2C_2O_4$ is getting excited under the UV light and decomposes into CO_2. During the decomposition, electrons are simultaneously transferred to Ag^+ ions to form Ag metal [21]. Absorption of UV light by $Ag_2C_2O_4$ is clear from the UV-visible DRS in Fig. 1. Formation of CO_2 has been confirmed by the appearance of white precipitate when the outlet of the reaction was passed through baryta $(Ba(OH)_2)$ solution [19]. Thus-formed Ag atoms nucleate after attaining a concentration and grow into

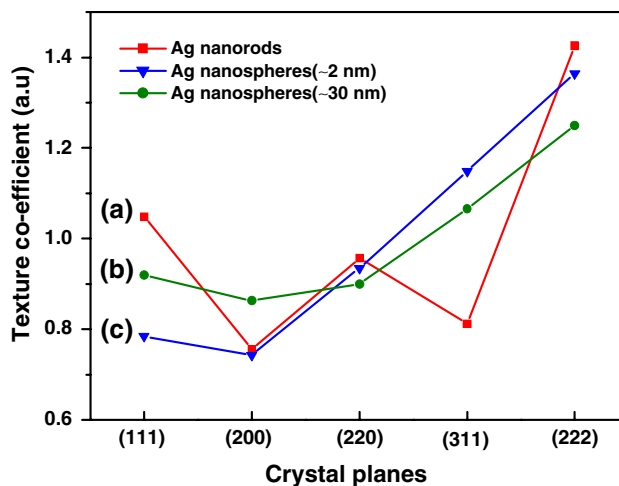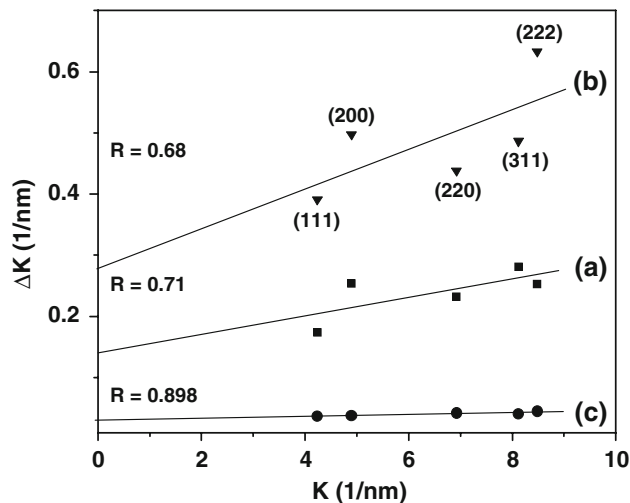Table 1 Parameters calculated from Williamson–Hall plot

Sample	Correlation coefficient (R)	Volume averaged crystallite size (D, nm)	Strain (ε)
Ag nanorods	0.71	7.2	0.0303
Ag nanospheres (1:5 of $Ag_2C_2O_4$ and PVP)	0.68	3.7	0.0646
Ag nanospheres (1:2 of $Ag_2C_2O_4$ and CTAB)	0.90	31.1	0.00156

particles. In the case of PVP as capping agent, formation of fine spherical particles only has been observed. This is due to the capping of PVP at all the crystal planes on Ag nuclei. Hence, faceting (anisotropic growth) of the crystals has not been observed. Formation of very fine particles (~ 2 nm) is due to the homogenous nucleation (yielding larger number of nuclei) followed by fast particle growth. Moreover, PVP, the macromolecular capping agent, prevents agglomeration of nanocrystals and makes the fine particles stable. However, in the case of CTAB as the capping agent (1:2 ratio of $Ag_2C_2O_4$ and CTAB), formation of spherical nanoparticles (~ 30 nm) has been observed. This is due to the poor capping ability of CTAB. Formation of nanorods in the case of 1:5 ratio of $Ag_2C_2O_4$ and CTAB is expected due to the suitable concentration of CTAB. Further increase in the concentration ratio (1:8) increases the length of the rods but featureless curvy nanorods are also observed. In general, formation of monodispersed Ag nanorods depends on the use of seed, pH of the medium, rate of the reduction of Ag^+ ions or rate of generation of Ag atoms, and concentration of CTAB [33]. Ascorbic acid is preferred as a reducing agent in the synthesis of Ag and Au nanorods. It is because ascorbic acid is a weak reducing agent and hence, the controlled generation of Ag atom occurs. It is because controlled generation of Ag atoms is necessary for the formation of monodispersed Ag nanorods [33]. In the current method, Ag nanoparticles first generated act as seeds as observed in HRTEM image (Fig. 6c). However, further particle growth is so fast due to the fast generation of Ag atoms in the growth solution out of the rapid decomposition. Hence, the rate of generation of Ag atoms from the decomposition is expected to have a major role in the formation of nanorods along with nanospheres (polydispersity). Since the rate of decomposition is directly proportional to the intensity of the UV lamp, low-intensity UV lamp may be suitable for the synthesis of monodispersed Ag nanorods. Apart from the role of CTAB for the formation of Ag nanorods, there is a possibility for the formation of worm-like Ag nanorods by the mere UV irradiation. This phenomenon is well known in silver halide photography where formation of Ag filaments occurs upon the UV irradiation on KBr microcrystals [34–36]. In such a case, small Ag nuclei formed on the surface of the silver halide microcrystals catalyze the reduction of Ag^+ ions present in silver halide microcrystals and give rise to the formation of Ag filaments. However, these Ag filaments degrade to small Ag nanoparticles (size <5 nm) upon further exposure to UV light over a period of time [37]. Hence, the effect of the UV irradiation is also responsible for the polydispersity of Ag nanoparticles and Ag nanorods obtained in the current method. In general, UV-visible irradiation on Ag and Au nanoparticles leads to the explosion of bigger particles into small clusters and the
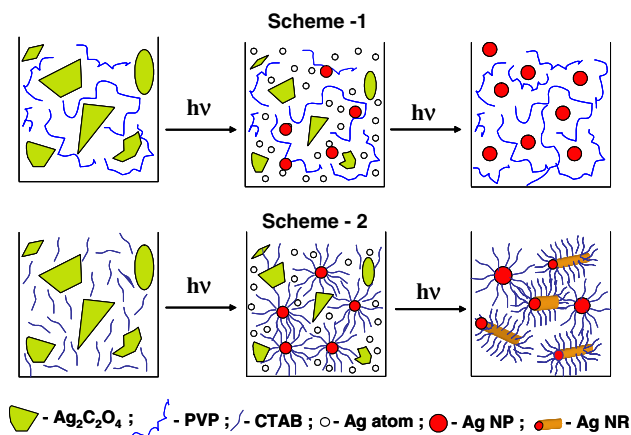

Fig. 12 Schematic representation of formation of (1) Ag nanospheres (using PVP) and (2) Ag nanorods (using CTAB)

sintering of the small clusters to bigger aggregates [37–39]. These two processes competitively occur in presence of UV-visible light. In such cases, defects are created in the resulting Ag nanocrystals due to the heating effect of UV-visible irradiation. This phenomenon is also possible in the current synthesis because Hg lamp employed possesses some amount of visible light also. Based on the above observations, formation mechanism has been explained schematically as shown in Fig. 12.

Conclusions

A fast synthesis of ultra-fine Ag nanospheres and nanorods has been demonstrated from silver oxalate in the presence of UV irradiation by using PVP and CTAB as capping agents, respectively. Spherical Ag nanoparticles of average size around 2 nm have been synthesized with 1:5 (w/w) ratio of $Ag_2C_2O_4$ and PVP. Ag nanorods of low aspect ratio have been obtained when ratio of $Ag_2C_2O_4$ and CTAB is 1:5 (w/w) in the absence of seed mediation. The preferential orientation of {111} facets has been observed in the case of nanorods. The monodispersity of the rods has not been achieved due to the fast generation of Ag atoms at the expense of $Ag_2C_2O_4$. Hence, utilization of low-intensity UV lamps may give rise to the formation of monodispersed Ag nanorods. The synthesized Ag nanoparticles with smaller size are found to contain more defects in lattice than those with the bigger size. The synthesized fine Ag nanospheres and the Ag nanorods can be potential candidates for catalysis and biocidal activities.

479

References

1. T. Vo-Dinh, F. Yan, M.B. Wabuyele, J. Raman Spectrosc. **36**, 640 (2005)
2. S. Schultz, D.R. Smith, J.J. Mock, D.A. Schultz, Proc. Natl Acad. Sci. USA **97**, 996 (2000). doi:10.1073/pnas.97.3.996
3. T.K. Jeorger, R. Jeorger, E. Olsson, C. Granqvist, Trends Biotechnol. **19**, 15 (2001). doi:10.1016/S0167-7799(00)01514-6
4. Q. Wu, H. Cao, Q. Luan, J. Zhang, Z. Wang, J.H. Warner, A.A.R. Watt, Inorg. Chem. **47**, 5882 (2008). doi:10.1021/ic8002228
5. S. Malynych, G. Chumanov, J. Opt, Pure Appl. Opt. **8**, S144 (2006). doi:10.1088/1464-4258/8/4/S14
6. H. Guo, S. Tao, Sens. Actuators B Chem. **123**, 578 (2007). doi:10.1016/j.snb.2006.09.055
7. I. Sondi, B.S. Sondi, J. Colloids Interface Sci. **275**, 177 (2004)
8. A. Dick, A.D. McFarland, C.L. Haynes, P.R.V. Duyne, J. Phys. Chem. B **106**, 853 (2002). doi:10.1021/jp013638l
9. K. Aslan, P. Holley, C.D. Geddes, J. Mater. Chem. **16**, 2846 (2006). doi:10.1039/b604650a
10. R.W.Y. Sun, R. Chen, N.P.Y. Chung, C.M. Ho, C.L.S. Lin, C.M. Che, Chem. Commun. **40**, 5059 (2005). doi:10.1039/b510984a
11. Y. Zhou, S.H. Yu, X.P. Cui, C.Y. Wang, Z.Y. Chen, Chem. Mater. **11**, 545 (1999). doi:10.1021/cm981122h
12. Y. Sun, Y. Xia, Adv. Mater. **14**, 833 (2002). doi:10.1002/1521-4095(20020605)14:11<833::AID-ADMA833>3.0.CO;2-K
13. M.H. Huang, A. Choudry, P.D. Yang, Chem Commun. 1063 (2000). doi:10.1039/b002549f
14. J. Sloan, D.M. Wright, H.G. Woo, S. Bailey, G. Brown, A.P.E. York, K.S. Coleman, J.L. Hutchison, M.L.H. Green, Chem Commun. 690 (1999)
15. C.J. Murphy, N.R. Jana, Adv. Mater. **14**, 80 (2002). doi:10.1002/1521-4095(20020104)14:1<80::AID-ADMA80>3.0.CO;2-#
16. J.Q. Hu, Q. Chen, Z.X. Xie, G.B. Han, R.H. Wang, B. Ren, Y. Zhang, Z.L. Yang, Z.Q. Tian, Adv. Funct. Mater. **14**, 183 (2004). doi:10.1002/adfm.200304421
17. G. Zhoua, M. Lu, Z. Yang, H. Zhang, Y. Zhou, S. Wang, S. Wang, A. Zhang, J. Cryst. Growth **289**, 255 (2006). doi:10.1016/j.jcrysgro.2005.11.106
18. K.K. Caswell, C.M. Bender, C.J. Murphy, Nano Lett. **3**, 667 (2003). doi:10.1021/nl0341178
19. S. Navaladian, B. Viswanathan, R.P. Viswanath, T.K. Varadarajan, Nanoscale Res. Lett. **2**, 44 (2007). doi:10.1007/s11671-006-9028-2
20. S. Navaladian, B. Viswanathan, T.K. Varadarajan, R.P. Viswanath, Nanotechnology **19**, 045603 (2008). doi:10.1088/0957-4484/19/04/045603
21. V.V. Boldyrev, Thermol. Chim. Acta **388**, 63 (2002)
22. X. Li, J. Zhang, W. Xu, H. Jia, X. Wang, B. Yang, B. Zhao, B. Li, Y. Ozaki, Langmuir **19**, 4285 (2003). doi:10.1021/la0341815
23. G.J. Lee, S.I. Shin, Y.C. Kim, S.G. Oh, Mater. Chem. Phys. **84**, 197 (2004). doi:10.1016/j.matchemphys.2003.11.024
24. V. Germain, J. Li, D. Ingert, Z.L. Wang, M.P. Pileni, J. Phys. Chem. B **107**, 8717 (2003). doi:10.1021/jp0303826
25. I. Washio, Y. Xiong, Y. Yin, Y. Xia, Adv. Mater. **18**, 1745 (2006). doi:10.1002/adma.200600675
26. B. Cullity, *Elements of X-ray Diffraction* (Addison-Wesley, Reading, MA, 1987)
27. S. Navaladian, C.M. Janet, B. Viswanathan, T.K. Varadarajan, R.P. Viswanath, J. Phys. Chem. C **111**, 14150 (2007). doi:10.1021/jp0744782
28. H. Wang, D.O. Northwood, Res. Lett. Mater. Sci. **2008**, 619032 (2008)
29. S. Navaladian, B. Viswanathan, T.K. Varadarajan, R.P. Viswanath, Nanoscale Res. Lett. **4**, 181 (2009). doi:10.1007/s11671-008-9223-4
30. G.K. Williamson, W.H. Hall, Acta Metall. **1**, 22 (1953). doi:10.1016/0001-6160(53)90006-6
31. Z. Yang, U. Welzel, Mater. Lett. **59**, 3406 (2005). doi:10.1016/j.matlet.2005.05.077
32. G. Milazzo, S. Caroli, V.K. Sharma, *Tables of Standard Electrode Potentials* (Wiley, Chichester, 1978)
33. C.J. Murphy, T.K. Sau, A.M. Gole, C.J. Orendorff, J. Gao, L. Gou, S.E. Hunyadi, T. Li, J. Phys. Chem. B **109**, 13857 (2005). doi:10.1021/jp0516846
34. D.C. Skillman, Photogr. Sci. Eng. **19**, 28 (1975)
35. G.S. Farnell, R.B. Flint, J. Photogr. Sci. **29**, 236 (1981)
36. V.N. Khvalyuk, A.L. Rogach, Proc. Belarus Acad. Sci. Chem. Ser. **3**, 67 (1993)
37. A.L. Rogach, G.P. Shevchenko, Z.M. Afanasev, V.V. Sviridov, J. Phys. Chem. B **101**, 8129 (1997). doi:10.1021/jp971350j
38. A. Takami, H. Kurita, S. Koda, J. Phys. Chem. B **103**, 1226 (1999). doi:10.1021/jp983503o
39. S. Link, Z.L. Wang, M.A. El-Sayed, J. Phys. Chem. B **104**, 7867 (2000). doi:10.1021/jp0011701